

See discussions, stats, and author profiles for this publication at: <https://www.researchgate.net/publication/279065086>

Water Mediated Interactions and the Protein Folding Phase Diagram in the Temperature–Pressure Plane

ARTICLE *in* THE JOURNAL OF PHYSICAL CHEMISTRY B · JUNE 2015

Impact Factor: 3.3 · DOI: 10.1021/acs.jpcb.5b03828 · Source: PubMed

CITATION

1

READS

19

3 AUTHORS, INCLUDING:



Nicholas P Schafer

Aarhus University

15 PUBLICATIONS 149 CITATIONS

[SEE PROFILE](#)

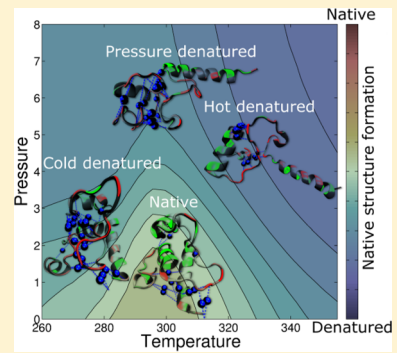
Water Mediated Interactions and the Protein Folding Phase Diagram in the Temperature–Pressure Plane

Brian J. Sirovetz,^{†,‡} Nicholas P. Schafer,^{†,§} and Peter G. Wolynes*,^{†,‡}

[†]Center for Theoretical Biological Physics, Rice University, 6500 Main Street, Houston, Texas 77030, United States

[‡]Department of Chemistry, Rice University, Space Science 201, Houston, Texas 77251, United States

ABSTRACT: The temperature–pressure behavior of two proteins, ubiquitin and λ -repressor, is explored using a realistically coarse-grained physicochemical model, the associative memory, water mediated, structure and energy model (AWSEM). The phase diagram across the temperature–pressure plane is obtained by perturbing the water mediated interactions in the Hamiltonian systematically. The phase diagrams calculated with direct simulations along with an extended bridge sampling estimator show the main features found experimentally, including both cold- and pressure-denaturation. The denatured ensembles in different parts of the phase diagram are characterized and found to be structurally distinct. The protein energy landscape is found to be funneled throughout the phase diagram, but modest changes in the entropy and free energy of the water are found to drive both cold and pressure induced denaturation.



INTRODUCTION

If proteins had evolved to fold in a vacuum, thermodynamic experiments in the laboratory could have been straightforwardly interpreted by statistical energy landscape theory, just as model computer simulations with implicit solvent have been.^{1–3} Instead, the intimate involvement of the aqueous environment in the folding process made the uncovering of the principles of the energy landscape theory of protein folding a convoluted process. When analyzed in detail, the experimental temperature/pressure phase diagram for protein folding has proved puzzling. One aspect of the phase diagram, that proteins lose their native properties at high temperature accompanied by an absorption of heat, was interpreted (correctly!) already in the 1930s by Mirsky and Pauling.⁴ *Prima facie*, as they understood, heat-denaturation of native proteins would seem to imply the native protein is much more ordered than the denatured state: Native proteins are folded... Great! Mirsky and Pauling recognized that a reasonably well-ordered protein structure would go far toward explaining the intricate specificity of biochemical interactions of native proteins, the hallmark of life at the molecular level, while denatured proteins by taking on a very large range of fluctuating structures would be promiscuous in their function. Yet some proteins also denature when they are cooled.⁵ Considering the second law of thermodynamics, how can this observed cold induced denaturation be reconciled with a folded protein being in an ordered state? Likewise, Bridgman discovered that proteins unfold when they are put under pressure.⁶ This observation also seems paradoxical since folded protein chains were found to be structurally compact by X-ray crystallography, while unfolded proteins in most ways seem to behave structurally like long disordered chains that would occupy a large volume. The observed high pressure induced denaturation from a compact state to one apparently

taking up more space thus also raises eyebrows. Nevertheless, physical chemists (especially those classically trained!) realized there was actually no contradiction of thermodynamics in these strange observations.^{7–11} Instead pressure and temperature act on the entire system of the protein molecule along with its aqueous environment. While the protein chain itself may expand and disorder when it unfolds, the surrounding solvent water can contract and order when a protein unfolds, and thereby, the protein makes a more intimate interface with its watery environment. The change of the entropy and volume of the interfacial water could account for the apparent paradox between structure changes and thermodynamics.

Simplified models having explicit solvent degrees of freedom have been shown to capture the key effects of cold denaturation.^{12–14} Much progress has also been made recently elucidating the basic molecular physics behind these unexpected protein denaturation processes using atomistic simulations.^{15–24} As in laboratory experiments, however, apportioning thermodynamic quantities between the chain and its environment along with the intrinsic complexity of fully atomistic models has led to some controversy in the interpretation of such simulations. At the same time, faithfully sampling the thermodynamic ensembles of fully atomistic models remains computationally challenging. Owing to this, comprehending the full range of structures found in specific proteins over the range of their folding phase diagrams is difficult even though here modern NMR techniques provide ample data for theoretical comparison.^{25,26} Furthermore, the kinetic

Special Issue: Biman Bagchi Festschrift

Received: April 21, 2015

Revised: June 16, 2015



ACS Publications

© XXXX American Chemical Society

A

DOI: 10.1021/acs.jpcb.5b03828
J. Phys. Chem. B XXXX, XXX, XXX–XXX

consequences of changes in the solvent-averaged interaction forces highlighted in model studies²⁷ remain unexplored in atomistic models despite their importance in the laboratory. Indeed fast folding experiments are often initiated from a cold-denatured ensemble whose structure must be known in order to account fully for the initial downhill folding events.^{28,29}

To complement the existing fully atomistic approaches to understanding the protein folding phase diagram, in this paper we aim to explore the thermodynamics of a coarse-grained but structurally and energetically realistic protein folding model that incorporates the changes in solvent-averaged interactions caused by temperature and pressure. Using coarse-grained models has several attractive features. Fairly complete thermodynamic ensemble sampling is well within available computational resources even for large systems when coarse-grained models are employed, while such extensive sampling is quite expensive when atomistic models are employed. The more complete sampling obtained using coarse-grained models allows explicit assessment of chain configurational entropy. Nailing down this contribution makes possible a clear apportionment of thermodynamic causes. Other tools of statistical energy landscape theory that are easily implemented for the coarse-grained models but that are more difficult to apply to atomistic models allow the degree of frustration, funneling, and ruggedness of the landscapes for chain motions to be assessed and eventually should permit kinetic predictions to be made.^{30,31} Finally, but certainly not least in importance, the transferable coarse-grained potential function we used was inferred using energy landscape theory in order to encode the “wisdom of the database”. This model has been shown to be able to predict both natural protein structures from sequence alone^{3,32} at moderate resolution and the detailed associations between protein molecules.³³ The AWSEM model also has been used to predict sometimes unexpected structural details of misfolded states of both designed and natural proteins.^{34–36} Thus, the structural consequences of solvent perturbations made to such a predictive force field should be taken with some seriousness.

The model we explore here starts with the AWSEM force field.³² AWSEM is a coarse-grained force field that has been optimized using energy landscape algorithms based on a database of solved protein structures. AWSEM stands for “associative memory, water mediated, structure, and energy model”. As its name implies, the interactions of the protein chain with water and through the solvent water are key elements of the force field. These transferable water mediated interactions were optimized for a database of proteins with known structure and sequence so as to make the energy landscape for these proteins as funneled as possible. Being based on a database of natural proteins, however, the interactions in the AWSEM force field reflect only the physical chemistry near physiological conditions. Our strategy for computing complete phase diagrams that must encompass temperatures and pressures that are far from physiological is then to add explicit temperature and pressure dependent perturbations to the zeroth order AWSEM force field inferred from the protein database. The form and magnitude of these perturbations reflect ideas highlighted in earlier work, especially the ideas on pressure effects in folding proposed by Garcia and Onuchic.²⁷ Those ideas were inspired by microscopic atomistic simulations and integral equation studies of the hydrophobic effect for model solutes in water.³⁷

Previously, Garcia and Onuchic studied the role of pressure on folding kinetics using a structure based model.²⁷ To represent the effects of pressure in their structure based model,

they introduced, instead of a simple contact term, a square well potential with a well and a barrier representing a solvent separated minimum and a barrier for desolvating residues, respectively. This additional desolvation barrier slows the formation of native contacts. The relative heights of the well and the barrier in that study were parametrized on the basis of the potential of mean force for methane in water that was obtained via an atomistic simulation.³⁷ The perturbations we make to the transferable AWSEM force field involving pressure are parametrized using these same simulation data.

In our calculations the change to the baseline water mediated interactions under physiological condition are taken to be uniform for all hydrophobic residues, while of course it is important that the zeroth order interactions in the AWSEM force fields are themselves heterogeneous and much more complex than those in a structure based model.

The perturbation strategy allows us not only to find structural ensembles at state points by direct simulation but also to use statistical mechanical perturbation theory to quickly scan the entire phase diagram. While only semiquantitative, the model reproduces the main features of the experimental phase diagrams of the two proteins, λ -repressor and ubiquitin. Both the direct simulations and the perturbation analyses allow us also to uncover the structural differences between denatured ensembles in different parts of the phase diagram. At the same time, the analysis shows that the protein energy landscape is funneled under all thermodynamic conditions and that only very modest changes from the energy landscape that has evolved under physiological conditions are needed in order to account for the complexity of the laboratory protein folding phase diagram in unusual conditions.

METHODS

Force Field. Simulations were carried out using the associative memory, water mediated, structure, and energy model (AWSEM). AWSEM is a coarse-grained protein force field that represents each residue using three explicit interaction sites (C_{α} , C_{β} , and O).³² AWSEM uses an implicit representation of the solvent by aliasing the effects of the solvent onto terms in the effective Hamiltonian. Although it is treated as a potential, AWSEM is, therefore, a solvent-averaged free energy function, not just an enthalpy term. Therefore, in principle, it should be temperature and pressure dependent. The solvent-averaged free energy terms used in the simulations for this study are given in eq 1.

$$V_{\text{AWSEM}} = V_{\text{backbone}} + V_{\text{contact}} + V_{\text{burial}} + V_{\text{HB}} + V_{\text{AM}} \quad (1)$$

The complete description of each of the terms in eq 1 can be found in the Supporting Information of a previous paper.³² Briefly, V_{backbone} consists of several harmonic pseudobonds that ensure the connectivity of the backbone, a chirality term that ensures correct stereochemistry, and a dihedral term for favoring protein-like torsional angles. V_{contact} accounts for tertiary interactions between residues and will be discussed further below. V_{burial} reflects a residue's preference to either be buried within the protein or to be exposed to solvent. V_{HB} includes both directional α -helical and cooperative β -hydrogen bonding terms. V_{AM} is the associative memory term, which is used to guide the formation of secondary structures. V_{AM} can be derived using bioinformatic alignments³² for the purposes of *de novo* structure prediction from sequences alone, but in the present physicochemical study of proteins whose native local structures are available, the associative memory term was

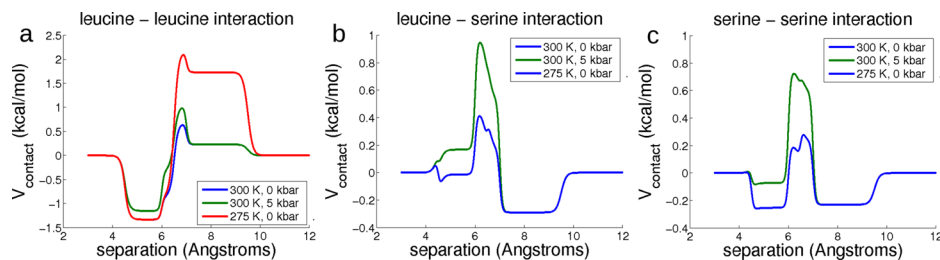


Figure 1. Plots of V_{contact} with $\Delta V_{\text{temperature}}(T)$ and $\Delta V_{\text{pressure}}(P)$ potentials added at several different temperatures and pressures for example pairs of (a) hydrophobic–hydrophobic residues, (b) hydrophobic–polar residues, and (c) polar–polar residues. For these plots $\sigma^{\text{wat}} = 1$.

obtained directly from the known experimental structure of each of the proteins: the local in-sequence interactions are strongly funneled.

The contact term eq 2 accounts for tertiary interactions between residues.

$$V_{\text{contact}} = V_{\text{direct}} + V_{\text{mediated}} \quad (2)$$

The parameters in this term have been optimized using energy landscape theory so as to maximize the ratio T_f/T_g for a database of training proteins.^{3,38–41} This ratio is obtained by maximizing the Z-score of the energy of native structures compared with the energies of molten globule structures sampled with the same Hamiltonian self-consistently. Maximizing T_f/T_g causes the landscape to be as funneled as it can be while the force field remains fully transferable. The contact potential in AWSEM is broken down into two interaction ranges. The direct contact portion acts on residues separated by 4.5–6.5 Å, while the protein/water mediated interactions are active at separations between 6.5 and 9.5 Å. Whether or not an interaction is considered to be protein mediated or water mediated depends on the density of other amino acids surrounding those residues at any time. If the local density of amino acids around both interacting residues is low, the interaction is considered to be water mediated ($\sigma^{\text{wat}} = 1$). If either or both of the interacting residues are buried, the interaction is considered to be protein mediated ($\sigma^{\text{wat}} = 0$). The potential switches smoothly from being protein mediated to water mediated for intermediate values of σ^{wat} , eq 3.

$$V_{\text{mediated}} = (1 - \sigma^{\text{wat}})V_{\text{protein}} + \sigma^{\text{wat}}V_{\text{water}} \quad (3)$$

The parameters in the AWSEM force field were obtained using a database of natural proteins that have evolved to fold in a relatively narrow range of physiological temperatures and pressures. The resulting parameters can be found in the Supporting Information of the original AWSEM-MD paper.³² In order to take into account the effect of nonphysiological temperatures and pressures on the free energy landscapes of the proteins, temperature and pressure dependent perturbations were added, independently, to the AWSEM tertiary interaction as shown in eq 4.

$$V_{\text{total}}(T, P) = V_{\text{AWSEM}} + \Delta V_{\text{temperature}}(T) + \Delta V_{\text{pressure}}(P) \quad (4)$$

To account for the environment induced changes in the relative interaction strengths between the protein and solvent, we introduced a temperature dependence to the water mediated interactions. The strength of the perturbation to the water mediated interactions varies linearly with temperature according to eq 5. In eq 5, Θ^{II} , σ^{wat} , and $\sigma^{\text{hydrophobes}}$ are switching functions which are equal to 1 if the interacting residues are within the mediated interaction range, have low local densities

of amino acids, and are hydrophobic residues, respectively, and equal to 0 otherwise. Detailed definitions of the switching functions Θ^{II} and σ^{wat} can be found in the Supporting Information of a previous paper.³² For the purposes of defining $\sigma^{\text{hydrophobes}}$, the following amino acids were considered to be hydrophobic: A, C, I, L, M, F, W, Y, V. The temperature variation parameters $m^{\text{temperature}}$ and $b^{\text{temperature}}$ were chosen to give reasonable cold- and hot-denaturation temperatures. For ubiquitin, the values of $m^{\text{temperature}} = -0.06 \text{ K}^{-1}$ and $b^{\text{temperature}} = 14.4$ were chosen. For λ -repressor, very similar values of $m^{\text{temperature}} = -0.06 \text{ K}^{-1}$ and $b = 18.6$ were chosen, again giving nearly the proper folded temperature range. As the temperature decreases, the well corresponding to solvent separated amino acid pairs involved in water mediated interactions between hydrophobic residues become deeper, and therefore such interactions become relatively more stable in comparison to the contact interaction. The contact potential for several different amino acid pairs is shown in Figure 1 at different temperatures.

$$\Delta V_{\text{temperature}}(T) = (m^{\text{temperature}} T + b^{\text{temperature}}) \Theta^{\text{II}} \sigma^{\text{wat}} \sigma^{\text{hydrophobes}} \quad (5)$$

In order to model the effects of high pressure, a pressure induced perturbation to the contact interaction is added as shown in eq 6. $\Delta V_{\text{pressure}}(P)$ consists of two pressure dependent perturbations. The first perturbation acts upon pairs of residues separated by 4.5–6.5 Å (Θ^{I}) and destabilizes direct contact interactions as pressure increases. The second perturbation is in the form of a barrier which increases in height as the pressure increases. The desolvation barrier acts upon pairs of residues that are separated by 6.0–7.0 Å and thereby disfavors configurations wherein a vacuum would form between the interacting residues due to the inability to fit a single water molecule between them. The parameters in $\Delta V_{\text{pressure}}(P)$ ($m_{\text{direct}}^{\text{pressure}}$, b_{direct} , $m_{\text{dsb}}^{\text{pressure}}$, and b_{dsb}) were adapted from a previous study of the desolvation barrier of methane pairs in water.³⁷ For the direct well, the parameters are $m_{\text{direct}}^{\text{pressure}} = 0.0361 \text{ kcal/kbar}$ and $b_{\text{direct}} = -0.353 \text{ kcal}$. For the desolvation barrier, the parameters are $m_{\text{dsb}}^{\text{pressure}} = 0.0726 \text{ kcal/kbar}$ and $b_{\text{dsb}} = 0.0461 \text{ kcal}$. The contact potential for several different pressures is shown in Figure 1.

$$\begin{aligned} \Delta V_{\text{pressure}}(P) = & (m_{\text{direct}}^{\text{pressure}} P + b_{\text{direct}}) \Theta^{\text{I}} \\ & + (m_{\text{dsb}}^{\text{pressure}} P + b_{\text{dsb}}) \Theta^{\text{dsb}} \end{aligned} \quad (6)$$

Order Parameters. The order parameter Q was used as an umbrella sampling coordinate and as a measure of native structure formation. The form of Q is given in eq 7, where r_{ij} is the instantaneous distance between the C_α atoms of residues i and j and r_{ij}^N is the same distance in the native structure. σ_{ij} is a weakly sequence separation dependent width.³² N_p is the number of unique pairs of residues satisfying the condition

$|i - j| > 2$, such that the Q values range from 0 (completely unfolded) to 1 (completely native).

$$Q = \frac{1}{N_p} \sum_{i-j>2} \exp\left(\frac{(r_{ij} - r_{ij}^N)^2}{2\sigma_{ij}^2}\right) \quad (7)$$

Using free energy profiles as a function of Q , threshold Q values were chosen for ubiquitin and λ -repressor (0.55 and 0.46, respectively) so as to distinguish between configurations belonging to the native ensemble from those in the denatured ensemble. ΔG_{f-u} , then, is the Gibbs free energy difference between these two subensembles ($\Delta G_{f-u} = G_{\text{folded}} - G_{\text{unfolded}}$) under a given set of conditions (T and P). The entropy change due to the degrees of freedom of the protein themselves, ΔS_{chain} , shown in eq 8, is simply the relative entropy difference between these ensembles, where ΔE is the difference of effective solvent-averaged potentials for the two subensembles ($\Delta E = E_{\text{folded}} - E_{\text{unfolded}}$).

$$\frac{\Delta S_{\text{chain}}}{k_B} = \frac{\langle \Delta E \rangle - \langle \Delta G_{f-u} \rangle}{k_B T} \quad (8)$$

Remember ΔE is itself a free energy since the effective interactions are already averaged over the solvent degrees of freedom: it is therefore temperature and pressure dependent. In contrast to ΔS_{chain} , the total entropy difference, ΔS_{total} , which includes entropy changes in the solvent, needs to be determined by numerically taking the derivative $\Delta S_{\text{total}} = -\frac{\partial \Delta G_{f-u}}{\partial T}$. The water entropy difference is then found by subtracting the chain entropy difference from the total entropy difference: $\Delta S_{\text{water}} = \Delta S_{\text{total}} - \Delta S_{\text{chain}}$.

We also monitor the radius of gyration, which is given by $R_g^2 = \sum_i (r_i - r_{\text{cm}})^2$ where r_i is the location of the C_α atom of residue i and r_{cm} is the location of the center of mass of the C_α atoms. To characterize where, within the protein, native structure is formed or disrupted locally, we compute Q_{local} , which is the fraction of native contacts instantaneously formed by a given single residue. The number of water mediated contacts is determined by counting the number of pairs of residues that satisfy the conditions $6.5 < r_{ij} < 9.5 \text{ \AA}$ and $\sigma^{\text{wat}} > 0.25$ in a given structure, where r_{ij} is the distance between C_β atoms of residues i and j (C_α in the case of glycine).

Sampling. To sample a wide range of configurations of ubiquitin and λ -repressor, umbrella sampling along Q was performed at multiple temperatures using the AWSEM model eq 1 along with Langevin dynamics as implemented in the LAMMPS⁴² molecular dynamics package. Many simulations were carried out using a harmonic bias to various fixed values of the structural similarity to the native folded form Q , eq 9.

$$V_{\text{bias}} = \frac{1}{2} k_{\text{bias}} (Q - Q^0)^2 \quad (9)$$

For each temperature (244 and 274 K for ubiquitin and 300, 320, and 340 K for λ -repressor), 17 different biased simulations were performed with Q^0 values ranging from 0.10 to 0.90, spaced evenly. Each of these simulations were run for 15 million steps with a time step of 2 fs, and configurations and energies were saved every 1000 steps.

Calculating Phase Diagrams. All free energies and expectation values were calculated using the multistate Bennet acceptance ratio (MBAR) as implemented in the pyMBAR package.⁴³ The MBAR method involves solving eq 10

self-consistently to obtain $\{\hat{f}_i\}$. In eq 10, j and k are the thermodynamic state indices, n is the sample index, and u is the reduced energy including the biasing potential, which is a function of the configuration \mathbf{x} .⁴³

$$\hat{f}_i = -\ln \sum_{j=1}^K \sum_{n=1}^{N_j} \frac{\exp[-u_i(\mathbf{x}_{jn})]}{\sum_{k=1}^K N_k \exp[\hat{f}_k - u_k(\mathbf{x}_{jn})]} \quad (10)$$

Once the set of $\{\hat{f}_i\}$ have been obtained from eq 10, unbiased free energies and expectation values of structural observables $A(\mathbf{x}_n)$ can then be estimated using eq 11 wherein u is now the reduced energy evaluated for the $V_{\text{total}}(T, P)$ of interest and does not include the biasing potential. Because the denominator in eq 10 does not change when unsampled states ($N_k = 0$) are added, no further self-consistent iteration is necessary, and eq 11 can be evaluated efficiently for all (T, P) of interest.

$$\hat{c}_A = \sum_{n=1}^N \frac{A(\mathbf{x}_n) \exp[-u(\mathbf{x}_n)]}{\sum_{k=1}^K N_k \exp[\hat{f}_k - u_k(\mathbf{x}_n)]} \quad (11)$$

$$\hat{c}_a = \sum_{n=1}^N \frac{\exp[-u(\mathbf{x}_n)]}{\sum_{k=1}^K N_k \exp[\hat{f}_k - u_k(\mathbf{x}_n)]} \quad (12)$$

$$\hat{A} = \frac{\hat{c}_A}{\hat{c}_a} \quad (13)$$

RESULTS

To test whether the present coarse-grained protein model based both on structural database information and physico-chemical input about how water interacts with amino acid pairs can explain the temperature–pressure unfolding behavior of proteins found in experiment, both temperature and pressure perturbations were computed for two well studied small systems, ubiquitin (PDBID: 1UBQ) and λ -repressor (PDBID: 1LMB). The phase diagrams were calculated by perturbing the temperature and pressure as outlined in the Methods section. The resulting phase diagrams are summarized in Figure 2 for ubiquitin and in Figure 5 for λ -repressor. Several quantities were calculated for each protein including the expected values of the fraction of native pairwise distances, Q , the number of water mediated contacts, and the radius of gyration, R_g . The chain energy and chain entropy profiles were computed under many thermodynamic conditions along with the total partial molar energy and entropy. The latter were obtained by differentiating the free energy profile.

The calculated phase diagrams for both ubiquitin and λ -repressor exhibit both hot- and cold-denaturation along with denaturation under high pressures. The plots of thermodynamic quantities and structural observables distinguish the native ensemble from the hot-, cold-, and pressure-denatured ensembles. Representative structures for each of the ensembles are shown in Figures 4 and 7.

Ubiquitin. The results for ubiquitin agree quite well with the picture gleaned from experimental studies. The nativeness of the protein as measured by the Q parameter decreases with both increasing and decreasing temperature as the temperature leaves the physiological range where the protein is natively folded (Figure 2a). The Q value at physiological conditions is 0.65, indicating that the protein adopts an ensemble of configurations very near to the average crystal structure. The nativeness at physiological conditions is further confirmed by

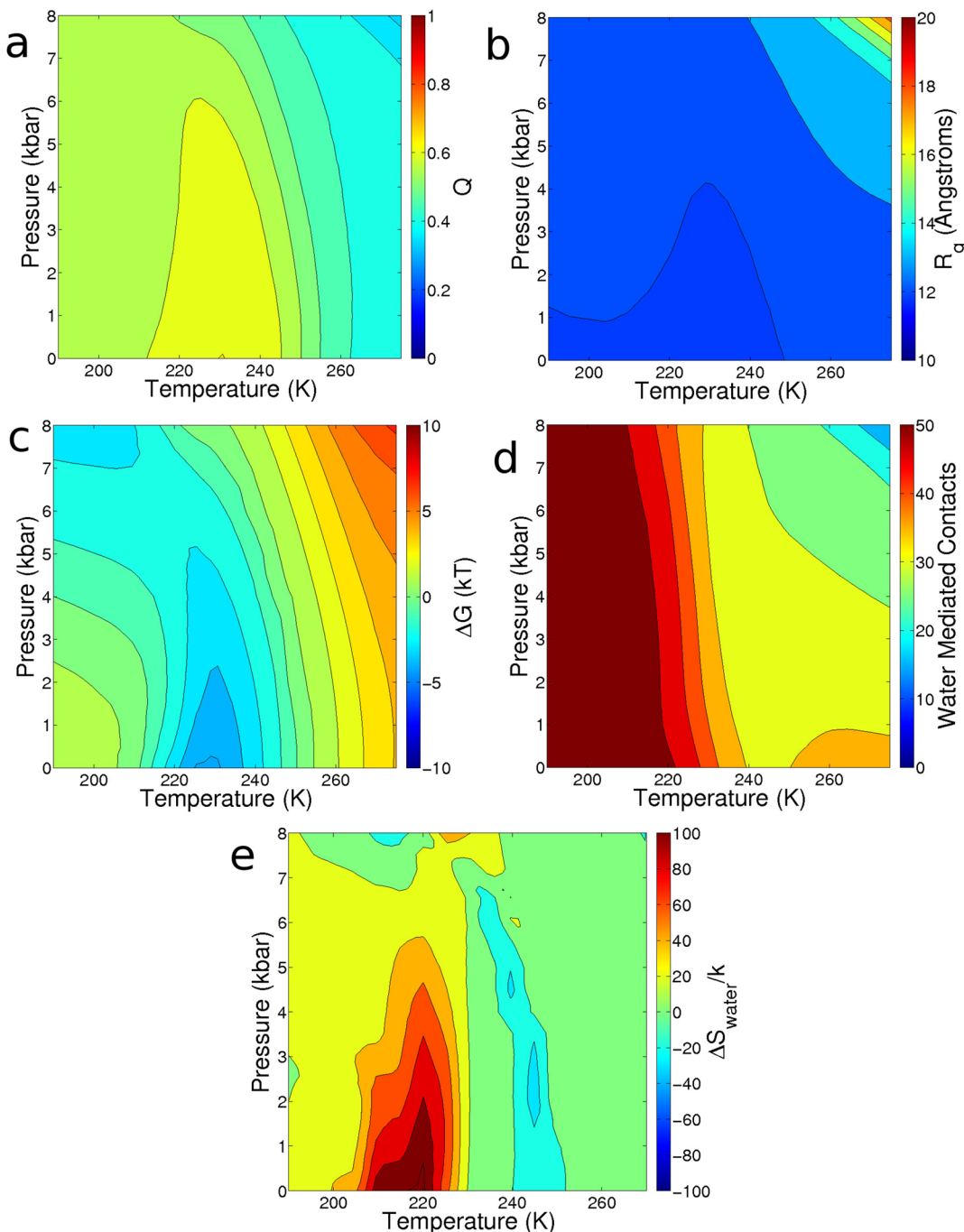


Figure 2. Temperature–pressure diagrams of ubiquitin for the quantities (a) $\langle Q \rangle$, (b) $\langle R_g \rangle$, (c) ΔG_{f-u} , (d) average water mediated contacts, and (e) $\Delta S_{water}/k_B$. The figures were obtained by perturbing the Hamiltonian to a variety of temperature and pressures on a fine grid. The plots were then obtained by linearly interpolating between the grid points.

measuring the fraction of native structure formed by each residue. If the fraction of native structure is close to 1, the local structure around that residue is native-like. Conversely, if the fraction of native structure is near 0, the local structure around the residue is not native-like. The fraction of native structure for each residue is shown visually in Figure 4a, where red represents a fraction close to 0 while green represents a fraction near to 1. The figure illustrates that the main structures in ubiquitin, the β -sheet and α -helix, have almost all of their native contacts formed, as shown in green. The areas which are missing native contacts, shown in red, are areas which are coils in the PDB structure. As the temperature decreases, the

protein unfolds partially, resulting in the Q parameter decreasing from 0.65 at 230 K to 0.5 at a temperature of 200 K. Similarly, as the temperature is increased, the protein also unfolds resulting in the Q parameter dropping from 0.65 to 0.4 at 270 K.

We now look at ΔG_{f-u} the free energy difference between the configurations belonging to the folded and unfolded ensembles ($\Delta G_{f-u} = G_{folded} - G_{unfolded}$). The ΔG_{f-u} phase diagram (Figure 2c) very much resembles the diagram calculated using the Q parameter. As the temperature departs from the physiological temperature range, the protein's native-like ensemble becomes destabilized. Unfolding results in ΔG_{f-u} switching from being

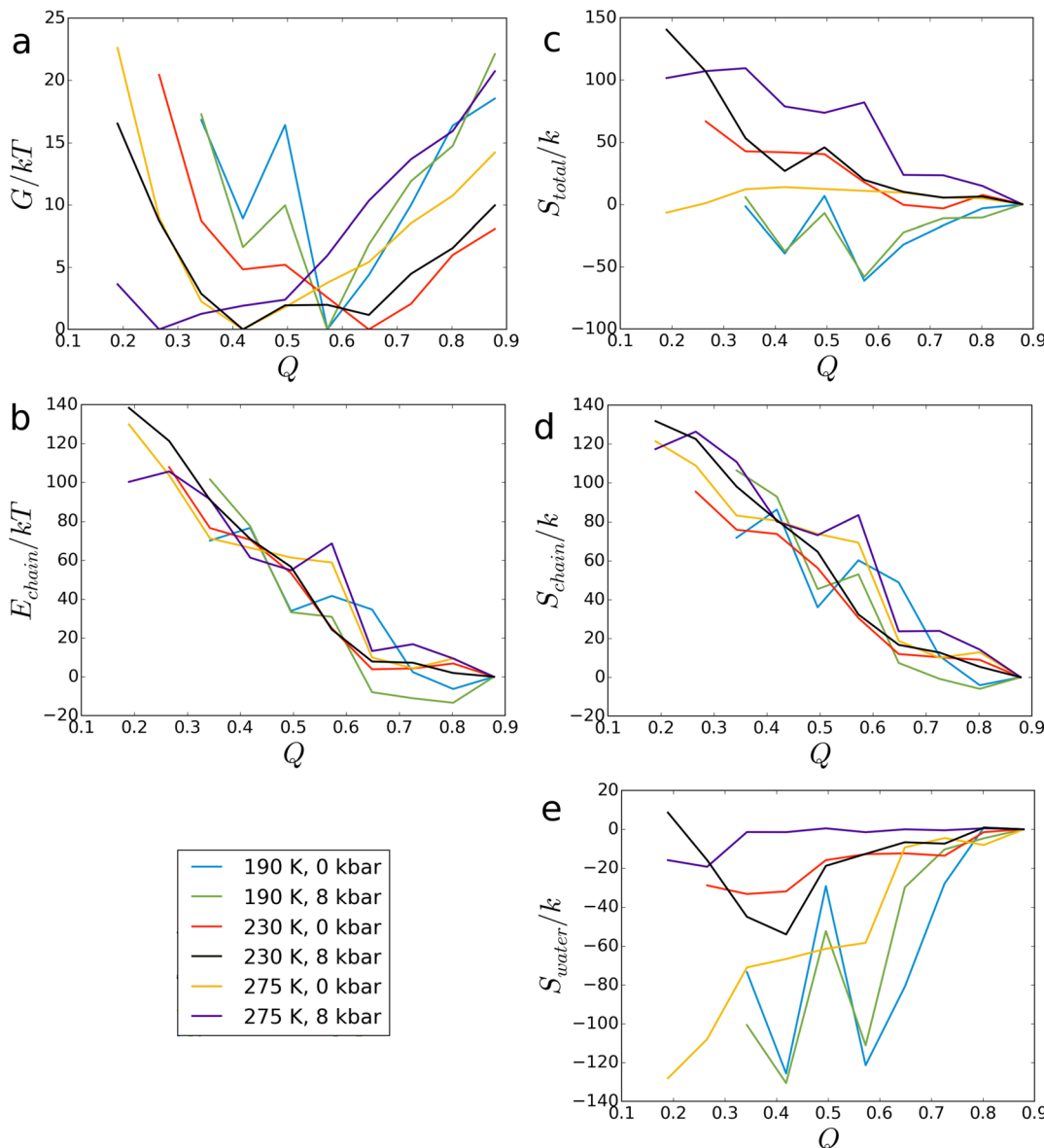


Figure 3. Plots of a variety of thermodynamic variables for ubiquitin as a function of the foldedness parameter Q for several different temperature and pressure conditions. The quantities (a) $G(Q)$, (b) $E_{chain}(Q)$, (c) $S_{total}(Q)$, (d) $S_{chain}(Q)$, and (e) $S_{water}(Q)$ are shown under the different conditions. Plots b–e were normalized such that the functions at $Q = 0.9$ are 0.

negative to being positive. At a temperature of 230 K the ΔG_{f-u} value is $-4kT$, indicating that the protein is stable in the native-like ensemble. As the temperature drops ΔG_{f-u} eventually changes sign. At 200 K ΔG_{f-u} is $1kT$, so the native-like ensemble is no longer favored. Conversely, as the temperature increases again, ΔG_{f-u} changes sign. At 270 K the ΔG_{f-u} value of $5kT$ indicates that the native ensemble is significantly destabilized. At low temperatures, as the pressure increases, ΔG_{f-u} becomes modestly more negative, which might suggest that the protein refolds under high pressure in this regime. While this type of behavior would be consistent with some previous simulations of helical peptides, the magnitude of this change in ΔG_{f-u} is small and almost certainly within the statistical error in the study.^{44–48}

It is difficult to distinguish between the native and denatured ensembles using the radius of gyration as a sole order parameter (Figure 2b). The R_g remains at a value of 12 Å under almost all of the temperatures and pressures shown. The only part of the phase diagram where the radius of gyration changes significantly

is when both temperature and pressure are high. The radius of gyration increases to a maximum value of 17 Å, indicating that at the highest temperatures the structure is expanded relative to the lower temperatures and pressures.

Plotting ΔS_{water} in the temperature–pressure plane helps highlight the important role water plays in the various types of denaturation (Figure 2e). Again, $\Delta S_{water} = \Delta S_{total} - \Delta S_{chain}$ where $\Delta S_{total} = -\frac{\partial \Delta G_{f-u}}{\partial T}$ and $\Delta S_{water} = \Delta S_{water(folded)} - \Delta S_{water(unfolded)}$. A positive value of ΔS_{water} indicates that the solvent becomes more structured in the unfolded state of the protein. Thus, at lower temperatures ($T < 230$ K), ΔS_{water} becomes positive. So the ordering of water tips the balance toward the unfolding of the protein. At higher temperatures, however, ΔS_{water} is nearly zero, indicating that the increase in chain entropy is primarily responsible for heat-denaturation of the protein.

Examining the thermodynamic functions $E_{chain}(Q)$ and $S_{chain}(Q)$ as a function of foldedness, Q , indicates that the protein

energy landscape is funneled under all of the temperature and pressure conditions shown, meaning that structures in the native ensemble have a considerably lower chain free energy and entropy compared to those belonging to denatured ensembles (Figure 3b,d). Even when global thermodynamics favors the denatured ensemble, the energy landscape is that of a minimally frustrated system.⁴⁹ Nevertheless, $S_{\text{water}}(Q)$ by itself does favor forming the folded state under all conditions. The general trend of S_{water} is to decrease as Q becomes lower (Figure 3e). For all conditions water orders around the chain as the protein denatures. Water entropy changes appear to drive cold denaturation.

An example of a structure found in the cold-denatured ensemble is shown in Figure 4d. Many more water mediated

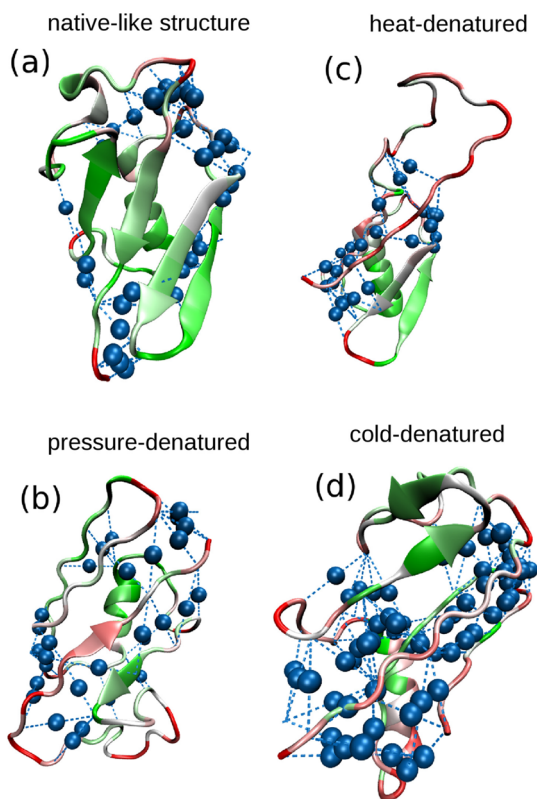


Figure 4. Representative structures of ubiquitin for several of the different ensembles: (a) native-like structure ($T = 230$ K and $P = 0$ kbar), (b) pressure-denatured structure ($T = 230$ K and $P = 8$ kbar), (c) heat-denatured structure ($T = 275$ K and $P = 0$ kbar), and (d) cold-denatured structure ($T = 190$ K and $P = 0$ kbar). Structures were rendered using VMD.⁵⁰

interactions are formed compared to what is found in the native-like structure. The locations of these interactions are indicated by the blue spheres representing the interstitial waters. The waters primarily disrupt the structure of the β -sheet, leaving the helix partially intact. The existence of a partially intact helix agrees with experiments that indicate that the regions that resist cold-denaturation the most are those around the N-terminal end of the α -helix.²⁵

While the temperature range where the folded ensemble is stable is tuned at the outset by setting the m and b parameters, the pressure range of stable folding is predicted from the model which assigns the pressure perturbations based on atomistic studies of methane in water. The pressure-denaturation of ubiquitin has been studied by Herberhold and Winter.⁵¹ Their study indicates

that ubiquitin denatures at about 5.9 kilobars at a temperature of 305 K, which is the peak on their inferred temperature-pressure phase diagram. In our simulations, we use $\Delta G_{f-u} = 0$ to precisely fix the pressure at which the protein denatures. Using the $\Delta G_{f-u} = 0$ criterion yields a peak unfolding pressure of 7.5 kilobars at a temperature of 230 K. Thus, the peak unfolding pressure is somewhat higher and the corresponding temperature lower than in experiment. The overpredicted peak pressure is likely due to the fact that many of the hydrophobic side chains in the protein are larger than the methane used to model the perturbation. The structural details of the pressure-denatured ensemble are more robust (Figure 4b). The predicted pressure-denatured structures can also be compared to previous work which studied the penetration of water under high pressure for ubiquitin via all atom simulations.⁵² Day, Paschek, and Garcia found that additional waters penetrated the structure under high pressure. The structure from our simulation shows that interpolating waters disrupt the β -sheet in the pressure-denatured ensemble. At high temperatures, the average number of water mediated contacts decreases with pressure from 35 at 0 kbar to 10 at 8 kbar as shown in Figure 2d. At lower temperatures, the average number of water mediated contacts shows little pressure dependence.

The heat-denatured ensemble (Figure 4c) is more expanded than the cold-denatured ensembles (Figure 4d). Nevertheless, the heat-denatured configuration contains much more structure than expected in a strict random coil. The structure around the helix remains particularly native-like as indicated by the fraction of native contacts formed by residues in the helix, which is represented by the green color in Figure 4. This residual structure may be enhanced by the associative memory term, which is highly funneled. The heat-denatured structure has an average of between 20 and 30 water mediated interactions compared to an average of 50 such interactions in the cold-denatured ensemble (Figure 2d).

λ -Repressor. Much as we have found for ubiquitin, λ -repressor in the present model also exhibits hot-, cold-, and pressure-denaturation. This behavior is clearly observed in the two-dimensional temperature-pressure plots of the foldedness parameter Q (Figure 5a) and the ΔG_{f-u} between folded and unfolded ensembles (Figure 5c). As the temperature departs from the physiological temperature of 300 K, Q decreases from 0.58 at 300 K to 0.45 at a temperature of 260 K and, also, upon heating there is a decrease from 0.58 to 0.30 at a temperature of 360 K. As pressure increases, the parameter Q decreases from 0.58 at physiological pressure to 0.30 at a pressure of 8 kbar, indicating a decrease in native structure.

To better assess the relative stability of the protein under the conditions we also compute the free energy difference between the folded and unfolded ensembles ($\Delta G_{f-u} = \Delta G_{\text{folded}} - \Delta G_{\text{unfolded}}$). ΔG_{f-u} being negative corresponds to the folded ensemble being more stable, whereas if ΔG_{f-u} is positive the denatured ensemble is favored. Again, we see that at physiological temperatures and pressures ΔG_{f-u} is negative, signaling the native ensemble is most stable (Figure 5c). If the temperature is either increased or decreased, however, the sign of ΔG_{f-u} eventually switches from negative to positive. Similarly, increasing the pressure away from physiological pressures also results in instability with ΔG_{f-u} becoming positive. We use the criterion $\Delta G_{f-u} = 0$ to precisely define the denaturation temperatures and pressures. For λ -repressor we find the temperature for heat-denaturation to be 325 K, and the peak pressure-denaturation to be 2.75 kbar.

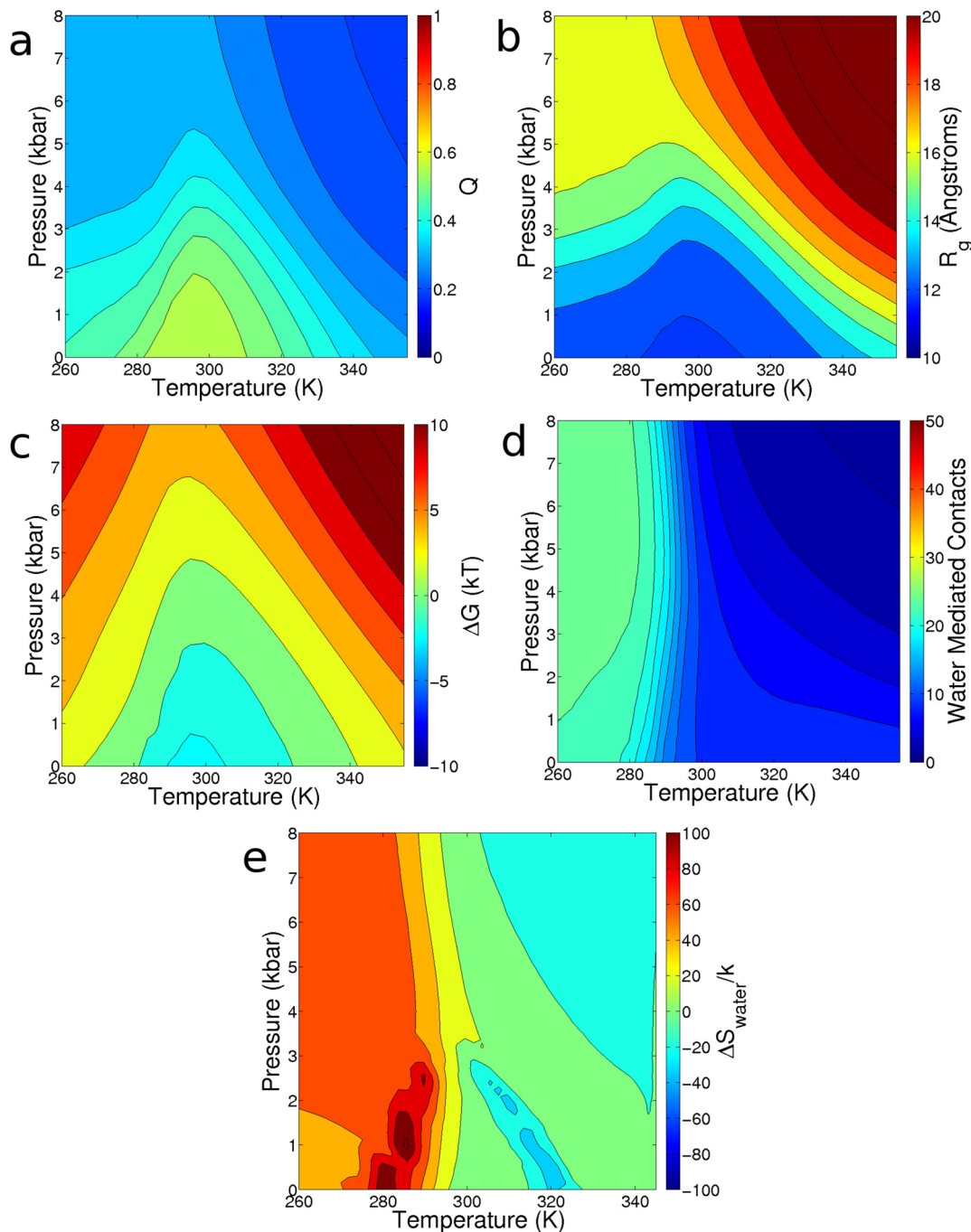


Figure 5. Temperature–pressure diagrams of λ -repressor for the quantities (a) $\langle Q \rangle$, (b) $\langle R_g \rangle$, (c) ΔG_{f-u} , (d) average water mediated contacts, and (e) ΔS_{water} . The figures were obtained by perturbing the Hamiltonian to a variety of temperature and pressures on a fine grid. The plots were then obtained by linearly interpolating between the grid points.

In this case the average radius of gyration phase diagram (Figure 5b) shows a strong resemblance to the average Q parameter diagram. The average radius of gyration increases with temperature once the physiological temperature is surpassed, changing from 11 Å at 300 K to 16 Å at 360 K. We see that the native ensemble is more compact than the heat-denatured ensemble, as is expected. On the other hand as the temperature decreases from the physiological temperature of 300 K, the average radius of gyration stays nearly constant at 11 Å. This suggests that the cold-denatured ensemble of λ -repressor is nearly as compact as the native ensemble. Increasing the pressure from 0 to 8 kbar results in

the average radius of gyration increasing from 11 to 17 Å suggesting that the pressure-denatured ensemble is expanded relative to the native ensemble.

To determine the role water plays in the various types of denaturations, we plot the temperature–pressure dependence of ΔS_{water} (Figure 5e) as we did for ubiquitin. Again, we use $\Delta S_{\text{water}} = \Delta S_{\text{total}} - \Delta S_{\text{chain}}$ where ΔS_{total} is obtained by numerically differentiating the free energy difference between the two ensembles: $\Delta S_{\text{total}} = -\frac{\partial \Delta G_{f-u}}{\partial T}$. When ΔS_{water} is positive, the solvent becomes more structured in the unfolded state, suggesting that water ordering contributes to the unfolding of

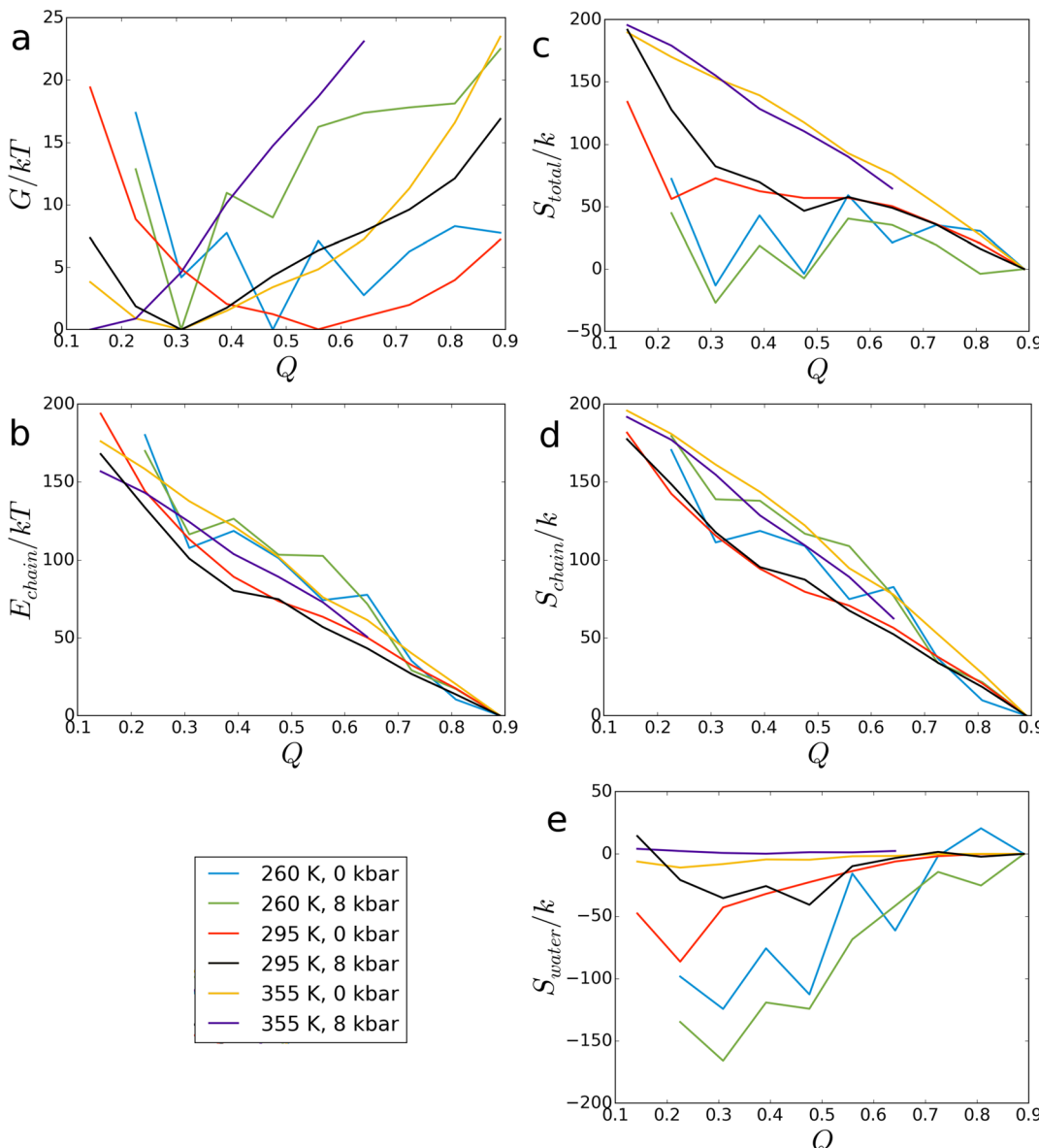


Figure 6. Plots of a variety of thermodynamic variables for λ -repressor as a function of the foldedness parameter Q for several different temperature and pressure conditions. The quantities (a) $G(Q)$, (b) $E_{\text{chain}}(Q)$, (c) $S_{\text{total}}(Q)$, (d) $S_{\text{chain}}(Q)$, and (e) $E_{\text{water}}(Q)/k_B$ are shown under the different conditions. Plots b–e were normalized such that the functions at $Q = 0.9$ are 0.

the protein chain. For λ -repressor, ΔS_{water} is positive at temperatures below 300 K indicating that the ordering of water drives cold-denaturation. Conversely, a negative ΔS_{water} indicates that water is less structured in the unfolded state. When the water entropy change is near zero, chain entropy must instead drive the protein denaturation, as is the case at higher temperatures.

We now look at several of the thermodynamic quantities as a function of the foldedness parameter Q , plotted in Figure 6. The solvent-averaged energy of the chain $E_{\text{chain}}(Q)$ strongly favors the folded state under both high and low temperatures and pressures. In other words, the energy landscape is always funneled, with E_{chain} decreasing as the structure becomes increasingly folded (Figure 6b). As expected, the entropy of the chain S_{chain} also decreases with increasing foldedness of the protein for low and high temperature and pressure conditions (Figure 6d). To assess the effect that water has in destabilizing the protein, we look at the water entropy, S_{water} , as a function of

the foldedness (Figure 6e). Here the water entropy is the difference between the total entropy and chain entropy at a particular Q value: $S_{\text{water}}(Q) = S_{\text{total}}(Q) - S_{\text{chain}}(Q)$. At low temperatures, S_{water} is lowest at low values of the foldedness parameter Q indicating that water becomes more ordered upon unfolding of the protein chain at lower temperatures. For higher temperatures, the water entropy is nearly constant as a function of Q , which means the chain entropy itself drives unfolding. The ordering of water around the unfolded protein chain at lower temperatures again highlights the key role that water plays in cold-denaturation of the protein chain.

Both the hot- and cold-denatured ensembles of λ -repressor maintain some helical structure as observed in Figure 7. The heat-denatured structures are more expanded compared to those in the cold-denatured ensemble, evidenced also by the higher values for the average R_g of these ensembles. Experimental work on λ -repressor by Huang and Oas suggests that the hot- and cold-denatured states are equivalent.⁵³

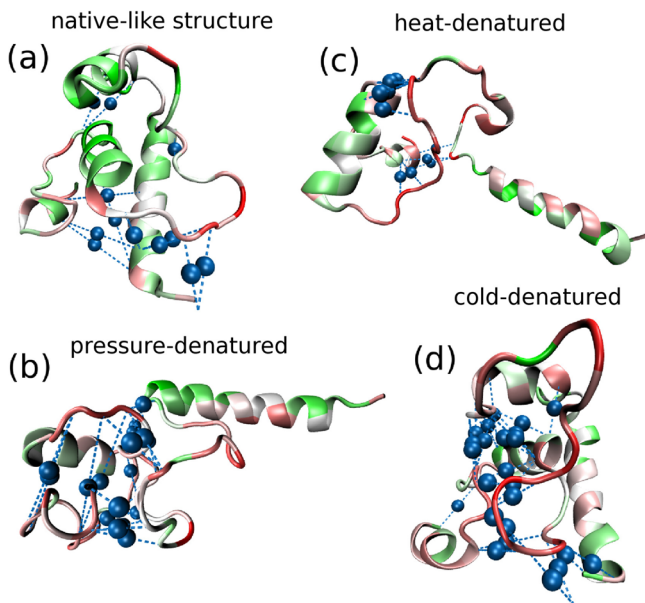


Figure 7. Representative structures of λ -repressor for several of the different ensembles: (a) native-like ($T = 300$ K and $P = 0$ kbar), (b) pressure-denatured ($T = 300$ K and $P = 8$ kbar), (c) heat-denatured ($T = 360$ K and $P = 0$ kbar), and (d) cold-denatured ($T = 260$ K and $P = 0$ kbar). Structures were rendered using VMD.⁵⁰

Huang and Oas however also conclude that the denatured states are random coils, suggesting the helical content was lost. This loss of helical content is not seen in our simulations which show that, while the hot- and cold-denatured ensembles are distinct, significant helical content still remains for both ensembles. Again this aspect of the prediction might be traced back to the strong funneling of the associative memory term. We also see that, at low temperatures, the average number of water mediated contacts is 30, and falls to 10 at high temperature (Figure 5d), suggesting the penetration of water at low temperatures.

The structures in the pressure-denatured ensemble of λ -repressor also reveal that helical content is present (Figure 7b). While there is less helical content in the pressure-denatured ensemble than in the native ensemble, two distinct helical regions remain. An atomistic molecular dynamics study on a mutant of λ -repressor by Schulten and Gruebele also indicated that the pressure-denatured ensemble contains almost as much helical content as the native ensemble.⁵⁴ Although the helical content found in the Gruebele and Schulten study does not agree perfectly with that found in our pressure-denatured ensemble, the fact that structures in both simulations show some similarity is encouraging.

Discussion. Scientists were aware of protein denaturation well before the structures of any proteins were resolved. It is not surprising that, as the temperature is increased, a protein will disorder and eventually unfold. Heat-denaturation is easily understood as being an entropy-driven process by which the compact ordered structure of a folded protein becomes disrupted, becoming noncompact and disordered.

While the existence of heat-denaturation of proteins may seem immediately intuitive, the existence of cold-denaturation is not. If the interactions between residues in proteins were completely enthalpic and thus constant at all temperatures and the landscape was highly funneled, one might expect proteins only to become increasingly ordered with decreasing

temperature. Yet cold-denaturation is far from rare for globular proteins. Cold-denaturation is instead largely entropically driven, resulting from changes in the solvent mediated interaction strengths as temperature changes. Even a modest weakening of the funneling is sufficient to tip the balance toward a denatured ensemble of configurations. This current study further confirms that altering interactions between the protein and water is sufficient to produce cold-denaturation and that a model incorporating such perturbations predicts structural changes upon denaturing consistent with experimental evidence.

Like cold-denaturation, understanding pressure-denaturation requires focusing on the interactions between the solvent and the protein. As the pressure is increased, water molecules are able to penetrate the hydrophobic core of the protein. As water penetrates, more numerous but weaker solvent separated interactions must hold the molecule together so the protein becomes increasingly susceptible to being denatured. Cavities in rigid proteins have also been invoked as providing a mechanism for pressure-denaturation. As the pressure rises, these cavities are thought to collapse resulting in denaturation of the protein.^{55,56} This scenario seems to be somewhat different from what occurs in this coarse-grained simulation. So while such an explanation based on cavities is not uniquely necessary, such an effect may also play a role in fine-tuning the phase diagram.

Proteins have evolved only to be able to function over relatively small temperature and pressure ranges. As a result, proteins need not be very stable in more extreme conditions than those the organism in which they reside would regularly encounter in nature. With the evolved nature of the folding landscape in mind, it is not surprising that proteins denature when the temperature and pressure depart significantly from the physiological range. The fine balance between chain entropy and energy on a funneled landscape need only be perturbed slightly to lead to denaturation. Proteins which are required to function at more extreme conditions can evolve to fold under those extreme conditions. A protein found in a hyperthermophilic organism has been found to have a melting temperature approaching 470 K, much higher than most proteins. Similarly, species which have evolved in cold conditions have antifreeze proteins which prevent the freezing solvent from causing harm. It will be interesting to study such extremophilic systems in the future using the present coarse-grained model.

CONCLUSIONS

We have used a physically motivated transferable protein force field that is accurate enough to predict protein structure from sequence in order to study the temperature–pressure stability of small proteins. The temperature–pressure space was scanned perturbatively to efficiently study a variety of temperature and pressure conditions.

We were able to calculate the temperature–pressure phase diagrams for ubiquitin and λ -repressor. The shapes of the phase diagrams are consistent with those measured experimentally, exhibiting hot, cold, and pressure induced denaturation in reasonable agreement with experimental phase diagrams. Additionally, the structures of the various denatured ensembles agree with many of the inferences from experimental studies.

The transitions predicted using the present model are less cooperative than folding transitions appear to be in experiment so it will be interesting to add other many body interactions in order to tune the cooperativity between secondary and tertiary structure formation.⁵⁷ This is particularly applicable to the heat-denatured structures shown, which show residual helical content with relatively little tertiary structure.

AUTHOR INFORMATION

Corresponding Author

*Phone: +1 713-348-4101. E-mail: pwolynes@rice.edu.

Present Address

[§](N.P.S.) iNANO, Aarhus University, Denmark.

Notes

The authors declare no competing financial interest.

ACKNOWLEDGMENTS

We are happy to dedicate this paper to Biman Bagchi whose contributions over several decades have shown the power of modern statistical mechanics not only to resolve classical problems but also to push forward the frontiers of chemistry. N.P.S. would like to thank Michael Shirts and John Chodera for their assistance with the MBAR method and pyMBAR software package. The project described was supported by Grant P01 GM071862 and Grant R01 GM44557 from the National Institute of General Medical Sciences. The content is solely the responsibility of the authors and does not necessarily represent the official views of National Institute of General Medical Sciences or the National Institutes of Health. Additional support was also provided by the D.R. Bullard-Welch Chair at Rice University, Grant C-0016.

REFERENCES

- (1) Bryngelson, J. D.; Onuchic, J. N.; Socci, N. D.; Wolynes, P. G. Funnels, Pathways, and the Energy Landscape of Protein Folding: a Synthesis. *Proteins: Struct., Funct., Bioinf.* **1995**, *21*, 167–195.
- (2) Shakhnovich, E. Protein Folding Thermodynamics and Dynamics: Where Physics, Chemistry, and Biology Meet. *Chem. Rev.* **2006**, *106*, 1559–1588.
- (3) Schafer, N. P.; Kim, B. L.; Zheng, W.; Wolynes, P. G. Learning to Fold Proteins Using Energy Landscape Theory. *Isr. J. Chem.* **2014**, *54*, 1311–1337.
- (4) Mirsky, A. E.; Pauling, L. On the Structure of Native, Denatured, and Coagulated Proteins. *Proc. Natl. Acad. Sci. U.S.A.* **1936**, *22*, 439.
- (5) Privalov, P. L. Cold Denaturation of Proteins. *Crit. Rev. Biochem. Mol. Biol.* **1990**, *25*, 281–306.
- (6) Bridgman, P. The Coagulation of Albumen by Pressure. *J. Biol. Chem.* **1914**, *19*, 511–512.
- (7) Kauzmann, W. Some Factors in the Interpretation of Protein Denaturation. *Adv. Protein Chem.* **1959**, *14*, 1–63.
- (8) Zipp, A.; Kauzmann, W. Pressure Denaturation of Metmyoglobin. *Biochemistry* **1973**, *12*, 4217–4228.
- (9) Weber, G.; Drickamer, H. G. The Effect of High Pressure Upon Proteins and Other Biomolecules. *Q. Rev. Biophys.* **1983**, *16*, 89–112.
- (10) Frye, K. J.; Royer, C. A. Probing the Contribution of Internal Cavities to the Volume Change of Protein Unfolding Under Pressure. *Protein Sci.* **1998**, *7*, 2217–2222.
- (11) Baldwin, R. L. Dynamic Hydration Shell Restores Kauzmann's 1959 Explanation of how the Hydrophobic Factor Drives Protein Folding. *Proc. Natl. Acad. Sci. U.S.A.* **2014**, *111*, 13052–13056.
- (12) Dias, C. L.; Ala-Nissila, T.; Karttunen, M.; Vattulainen, I.; Grant, M. Microscopic Mechanism for Cold Denaturation. *Phys. Rev. Lett.* **2008**, *100*, 118101.
- (13) Dias, C. L. Unifying Microscopic Mechanism for Pressure and Cold Denaturations of Proteins. *Phys. Rev. Lett.* **2012**, *109*, 048104.
- (14) Matysiak, S.; Debenedetti, P. G.; Rossky, P. J. Role of Hydrophobic Hydration in Protein Stability: A 3D Water-Explicit Protein Model Exhibiting Cold and Heat Denaturation. *J. Phys. Chem. B* **2012**, *116*, 8095–8104.
- (15) Bandyopadhyay, S.; Chakraborty, S.; Bagchi, B. Coupling Between Hydration Layer Dynamics and Unfolding Kinetics of HP-36. *J. Chem. Phys.* **2006**, *125*, 084912.
- (16) Paschek, D.; Hempel, S.; García, A. E. Computing the Stability Diagram of the Trp-Cage Miniprotein. *Proc. Natl. Acad. Sci. U.S.A.* **2008**, *105*, 17754–17759.
- (17) Lopez, C. F.; Darst, R. K.; Rossky, P. J. Mechanistic Elements of Protein Cold Denaturation. *J. Phys. Chem. B* **2008**, *112*, 5961–5967.
- (18) Chakrabarty, S.; Bagchi, B. Temperature Dependent Free Energy Surface of Polymer Folding from Equilibrium and Quench Studies. *J. Chem. Phys.* **2010**, *133*, 214901.
- (19) Day, R.; Paschek, D.; Garcia, A. E. Microsecond Simulations of the Folding/Unfolding Thermodynamics of the Trp-Cage Miniprotein. *Proteins: Struct., Funct., Bioinf.* **2010**, *78*, 1889–1899.
- (20) Okumura, H. Temperature and Pressure Denaturation of Chignolin: Folding and Unfolding Simulation by Multibaric-Multi-thermal Molecular Dynamics Method. *Proteins: Struct., Funct., Bioinf.* **2012**, *80*, 2397–2416.
- (21) Roy, S.; Bagchi, B. Comparative Study of Protein Unfolding in Aqueous Urea and Dimethyl Sulfoxide Solutions: Surface Polarity, Solvent Specificity, and Sequence of Secondary Structure Melting. *J. Phys. Chem. B* **2014**, *118*, 5691–5697.
- (22) Yang, C.; Jang, S.; Pak, Y. A Fully Atomistic Computer Simulation Study of Cold Denaturation of a β -Hairpin. *Nat. Commun.* **2014**.
- (23) Ghosh, R.; Roy, S.; Bagchi, B. Multidimensional Free Energy Surface of Unfolding of HP-36: Microscopic Origin of Ruggedness. *J. Chem. Phys.* **2014**, *141*, 135101.
- (24) English, C. A.; García, A. E. Folding and Unfolding Thermodynamics of the TC10b Trp-Cage Miniprotein. *Phys. Chem. Chem. Phys.* **2014**, *16*, 2748–2757.
- (25) Babu, C. R.; Hilser, V. J.; Wand, A. J. Direct Access to the Cooperative Substructure of Proteins and the Protein Ensemble via Cold Denaturation. *Nat. Struct. Mol. Biol.* **2004**, *11*, 352–357.
- (26) Vajpai, N.; Nisius, L.; Wiktor, M.; Grzesiek, S. High-Pressure NMR Reveals Close Similarity Between Cold and Alcohol Protein Denaturation in Ubiquitin. *Proc. Natl. Acad. Sci. U.S.A.* **2013**, *110*, E368–E376.
- (27) Hillson, N.; Onuchic, J. N.; García, A. E. Pressure-Induced Protein-Folding/Unfolding Kinetics. *Proc. Natl. Acad. Sci. U.S.A.* **1999**, *96*, 14848–14853.
- (28) Ballew, R.; Sabelko, J.; Gruebele, M. Direct Observation of Fast Protein Folding: the Initial Collapse of Apomyoglobin. *Proc. Natl. Acad. Sci. U.S.A.* **1996**, *93*, 5759–5764.
- (29) Sabelko, J.; Ervin, J.; Gruebele, M. Cold-Denatured Ensemble of Apomyoglobin: Implications for the Early Steps of Folding. *J. Phys. Chem. B* **1998**, *102*, 1806–1819.
- (30) Ferreiro, D. U.; Hegler, J. A.; Komives, E. A.; Wolynes, P. G. Localizing Frustration in Native Proteins and Protein Assemblies. *Proc. Natl. Acad. Sci. U.S.A.* **2007**, *104*, 19819–19824.
- (31) Jenik, M.; Parra, R. G.; Radusky, L. G.; Turjanski, A.; Wolynes, P. G.; Ferreiro, D. U. Protein Frustrometer: a Tool to Localize Energetic Frustration in Protein Molecules. *Nucleic Acids Res.* **2012**, *40*, W348–W351.
- (32) Davtyan, A.; Schafer, N. P.; Zheng, W.; Clementi, C.; Wolynes, P. G.; Papoian, G. A. AWSEM-MD: Protein Structure Prediction Using Coarse-Grained Physical Potentials and Bioinformatically Based Local Structure Biasing. *J. Phys. Chem. B* **2012**, *116*, 8494–8503.
- (33) Zheng, W.; Schafer, N. P.; Davtyan, A.; Papoian, G. A.; Wolynes, P. G. Predictive Energy Landscapes for Protein-Protein Association. *Proc. Natl. Acad. Sci. U.S.A.* **2012**, *109*, 19244–19249.
- (34) Truong, H. H.; Kim, B. L.; Schafer, N. P.; Wolynes, P. G. Funneling and Frustration in the Energy Landscapes of Some Designed and Simplified Proteins. *J. Chem. Phys.* **2013**, *139*, 121908.
- (35) Zheng, W.; Schafer, N. P.; Wolynes, P. G. Frustration in the Energy Landscapes of Multidomain Protein Misfolding. *Proc. Natl. Acad. Sci. U.S.A.* **2013**, *110*, 1680–1685.
- (36) Zheng, W.; Schafer, N. P.; Wolynes, P. G. Free Energy Landscapes for Initiation and Branching of Protein Aggregation. *Proc. Natl. Acad. Sci. U.S.A.* **2013**, *110*, 20515–20520.
- (37) Hummer, G.; Garde, S.; García, A. E.; Paulaitis, M. E.; Pratt, L. R. The Pressure Dependence of Hydrophobic Interactions is

- Consistent with the Observed Pressure Denaturation of Proteins. *Proc. Natl. Acad. Sci. U.S.A.* **1998**, *95*, 1552–1555.
- (38) Hardin, C.; Eastwood, M. P.; Prentiss, M. C.; Luthey-Schulten, Z.; Wolynes, P. G. Associative Memory Hamiltonians for Structure Prediction Without Homology: α/β Proteins. *Proc. Natl. Acad. Sci. U.S.A.* **2003**, *100*, 1679–1684.
- (39) Hardin, C.; Eastwood, M. P.; Luthey-Schulten, Z.; Wolynes, P. G. Associative Memory Hamiltonians for Structure Prediction Without Homology: Alpha-Helical Proteins. *Proc. Natl. Acad. Sci. U.S.A.* **2000**, *97*, 14235–14240.
- (40) Koretke, K. K.; Luthey-Schulten, Z.; Wolynes, P. G. Self-Consistently Optimized Energy Functions for Protein Structure Prediction by Molecular Dynamics. *Proc. Natl. Acad. Sci. U.S.A.* **1998**, *95*, 2932–2937.
- (41) Papoian, G. A.; Ulander, J.; Wolynes, P. G. Role of Water Mediated Interactions in Protein-Protein Recognition Landscapes. *J. Am. Chem. Soc.* **2003**, *125*, 9170–9178.
- (42) Plimpton, S. Fast Parallel Algorithms for Short-Range Molecular Dynamics. *J. Comput. Phys.* **1995**, *117*, 1–19.
- (43) Shirts, M. R.; Chodera, J. D. Statistically Optimal Analysis of Samples from Multiple Equilibrium States. *J. Chem. Phys.* **2008**, *129*, 124105.
- (44) Takekiyo, T.; Shimizu, A.; Kato, M.; Taniguchi, Y. Pressure-Tuning FT-IR Spectroscopic Study on the Helix-Coil Transition of Ala-Rich Oligopeptide in Aqueous Solution. *Biochim. Biophys. Acta, Proteins Proteomics* **2005**, *1750*, 1–4.
- (45) Mori, Y.; Okumura, H. Pressure-Induced Helical Structure of a Peptide Studied by Simulated Tempering Molecular Dynamics Simulations. *J. Phys. Chem. Lett.* **2013**, *4*, 2079–2083.
- (46) Mori, Y.; Okumura, H. Molecular Dynamics of the Structural Changes of Helical Peptides Induced by Pressure. *Proteins: Struct., Funct., Bioinf.* **2014**, *82*, 2970–2981.
- (47) Hatch, H. W.; Stillinger, F. H.; Debenedetti, P. G. Computational Study of the Stability of the Miniprotein Trp-Cage, the GB1 β -Hairpin, and the AK16 Peptide, Under Negative Pressure. *J. Phys. Chem. B* **2014**, *118*, 7761–7769.
- (48) Best, R. B.; Miller, C.; Mittal, J. Role of Solvation in Pressure-Induced Helix Stabilization. *J. Chem. Phys.* **2014**, *141*, 22D522.
- (49) Bryngelson, J. D.; Wolynes, P. G. Spin Glasses and the Statistical Mechanics of Protein Folding. *Proc. Natl. Acad. Sci. U.S.A.* **1987**, *84*, 7524–7528.
- (50) Humphrey, W.; Dalke, A.; Schulten, K. VMD - Visual Molecular Dynamics. *J. Mol. Graphics* **1996**, *14*, 33–38.
- (51) Herberhold, H.; Winter, R. Temperature-and Pressure-Induced Unfolding and Refolding of Ubiquitin: a Static and Kinetic Fourier Transform Infrared Spectroscopy Study. *Biochemistry* **2002**, *41*, 2396–2401.
- (52) Day, R.; García, A. E. Water Penetration in the Low and High Pressure Native States of Ubiquitin. *Proteins: Struct., Funct., Bioinf.* **2008**, *70*, 1175–1184.
- (53) Huang, G. S.; Oas, T. G. Heat and Cold Denatured States of Monomeric λ Repressor are Thermodynamically and Conformationally Equivalent. *Biochemistry* **1996**, *35*, 6173–6180.
- (54) Liu, Y.; Prigozhin, M. B.; Schulten, K.; Gruebele, M. Observation of Complete Pressure-Jump Protein Refolding in Molecular Dynamics Simulation and Experiment. *J. Am. Chem. Soc.* **2014**, *136*, 4265–4272.
- (55) Roche, J.; Caro, J. A.; Norberto, D. R.; Barthe, P.; Roumestand, C.; Schlessman, J. L.; Garcia, A. E.; Garcia-Moreno, B.; Royer, C. A. Cavities Determine the Pressure Unfolding of Proteins. *Proc. Natl. Acad. Sci. U.S.A.* **2012**, *109*, 6945–6950.
- (56) Lassalle, M. W.; Yamada, H.; Morii, H.; Ogata, K.; Sarai, A.; Akasaka, K. Filling a Cavity Dramatically Increases Pressure Stability of the c-Myb R2 Subdomain. *Proteins: Struct., Funct., Bioinf.* **2001**, *45*, 96–101.
- (57) Eastwood, M. P.; Wolynes, P. G. Role of Explicitly Cooperative Interactions in Protein Folding Funnels: a Simulation Study. *J. Chem. Phys.* **2001**, *114*, 4702–4716.